AIAA JOURNAL
Vol. 42, No. 10, October 2004

Nonlinear Development of Particle-Laden Mixing Layers at Low Mach Number

N. Thevand* and E. Daniel†
Institut Universitaire des Systèmes Thermiques Industriels, 13453 Marseille Cedex 13, France

The two-phase coupling effects on the particle-laden compressible mixing layer are studied for low convective Mach numbers. A full Eulerian approach is used to obtain a set of conservative partial differential equations. The initial condition is provided by the solution of the solution of the linear problem. The numerical solutions show that the presence of particles in the flow does not alter the typical development of the mixing layer observed for one-phase flows: the amplification of linear instability waves, the formation of two-dimensional large-scale vortices, and the pairing of vortices. The shape of the vortical structures is modified compared to single-phase calculations. The particle density distribution is greatly dependant on their inertia that can lead to a particle-free zone in the vortex. The compressibility effects are clearly seen on the modal kinetic energy, which decreases when the convective Mach number increases. The two-phase coupling effects on the modal kinetic energy of a coherent structure are found to be more important when the ratio of the particle relaxation time on the specific development time of this structure is close to unity, and these effects are lower for low and large ratios.

Nomenclature

a	=	sound speed, m/s
Cv, Cp	=	heat capacity at constant volume or constant pressure, J/(kg · K)
$\bar{\bar{I}}_d$	=	identity tensor
P	=	gas pressure, Pa
Pr	=	Prandtl number for a spherical particle in gas
R	=	gas constant, J/(kg · K)
Re_p	=	particle Reynolds number, $\rho\|\boldsymbol{u} - \boldsymbol{u}_p\|d_p/\mu$
T	=	temperature, K
$\boldsymbol{u}$	=	velocity vector, m/s
α_p	=	volume fraction of the dispersed phase
κ_t	=	thermal conductivity of the gas phase, W/(m · K)
ρ	=	density, kg/m^3

Subscripts

f	=	fundamental mode
k	=	continuous-phase indicator
p	=	particle (dispersed) phase

Introduction

THE study of the development of the two-phase, dilute gas particles, compressible mixing layer flow has been motivated by the need of knowledge of the interaction between aluminium particles and the gas vortical structures developing in the internal flow of solid rocket motors: The vortex-shedding occurring is these motors can lead to severe damages, and an accurate understanding of this phenomenon is needed. In a more general way, this kind of flow can be found in many industrial and energy-related processes, including combustion of fuel sprays and high-energy solid compounds or chemical reactant mixing. Beyond these industrial applications, the particle-laden mixing layer study still represents an important basis for understanding the two phase influence on the development of instabilities.

The particles/mixing layer interaction can be characterized by the stabilization of the flow and also by the particles dispersion in the vortices.

Saffman[1] and Michael[2] carried out early numerical studies on two-way coupling effects on the stability of particle-laden mixing layers. Saffman[1] found that the addition of particles with a small relaxation time tends to destabilize the flow, whereas, the addition of large-inertia particles stabilizes the flow. At finite Reynolds flow ($Re < 500$), the numerical investigation of Tong and Wang[3] on the mixing layer linear development confirmed these asymptotic relations. Michael[2] studied the linear development of a perturbation in an inviscid incompressible particle-laden mixing layer flow and showed that particles always stabilize the flow. The same conclusion was reached by Yang et al.,[4] who integrated numerically a modified Rayleigh instability equation for an inviscid incompressible spatially evolving mixing layer with different particle loadings.

Experimental[5–7] and computational[8] investigations have been conducted to understand the basic mechanism of the dispersion of particles by large-scale vortical structures. A physical model based on the interactions of particles with the large-scale vortices has been developed by Crowe et al.[9] The central idea of this model is that the Stokes number St defined as the ratio of the particle dynamic relaxation time to the flow characteristic time, governs the particle dispersion. For Stokes number much smaller than unity, the particles follow the fluid motion. For Stokes number larger than unity, the particles are little affected by the gas flow and disperse at low rates. On the contrary, particles with a Stokes number of the order of unity disperse at larger rates. In the case, the particles are centrifuged from the vortex cores and accumulate in the periphery of large-scale vortices.

When the nonlinear development of particle laden mixing layers is studied, the assumption of dilute flows is retained in most works, and this assumption is associated with a one-way modeling of the flow. This means that the effects of the particles on the carrier phase are neglected. Consequently, few investigations address the effects of two-way coupling on this kind of mixing layers. One can refer to the work of Wang et al.,[10] who simulate two-phase incompressible flows. They showed that two-way coupled particle-laden mixing layers also undergo rollup and subsequent vortex pairing, but the presence of the particles alters the structure of the rollup vortices in a way that depends on the particle inertia, which demonstrates the importance of the retroactive effects of the particles on the gas phase.

Received 31 December 2002; accepted for publication 26 September 2003.

*Postdoctoral Researcher, UMR, Centre National de la Recherche Scientifique 6595, Technopôle de Château Gombert, 5, rue Enrico Fermi.

†Professor, UMR, Centre National de la Recherche Scientifique 6595, Technopôle de Château Gombert, 5, rue Enrico Fermi; also Professor, Project SMASH, Institut National de Recherche en Informatique et Automatique, 06902 Sophia Antipolis, France; eric.daniel@polytech.univ-mrs.fr.

The effects of the compressibility of the carrier phase have been little studied for two-phase mixing layers. Miller and Bellan[11] present a study of a mixing layer with one laden stream with evaporating particles by performing direct numerical simulations of the flow, including a two-way coupling model. Although the gas obeys the ideal gas law, the compressibility effects are not systematically investigated. A work was initiated in this way[12] by considering the influence of fluid/particles interactions on the linear development of a mixing layer. The results have shown that the stabilization effects of the particles on the perturbation development increase with the influence of compressibility (for low Mach number). The product of the wave number of the perturbation, α, and the Stokes number St was pointed out to be a pertinent to characterize the role of the particle inertia, whatever the convective Mach number. The stabilization mechanism reaches a peak for $\alpha \mathrm{St} \approx 1$. It was also established that the dispersed phase favors the development of three-dimensional instability at lower Mach number than for one-phase flows. The study of the gas vorticity eigenfunctions showed important differences between particle-laden flows and single-phase flows, depending on particle inertia and the compressibility effects.

The nonlinear temporal development of two-dimensional mixing layers is here studied, based on the numerical solutions of the governing equations of the dilute two-phase inviscid compressible flow. A full Eulerian–Eulerian approach is chosen instead of Eulerian–Lagrangian models generally used. The choice of an Eulerian–Eulerian model is motivated by that the source terms in the system of equations, related to the two-way coupling phenomena (drag force, heat exchange), appear naturally in the equations and their numerical integration is easier without any interpolation of the numerical solution. The set of partial differential equations is then solved with a second-order finite volume scheme based on exact Riemann solvers. With this combination, high computing resources are not required to obtained numerical solutions. A specific difficulty is due to the initial condition that must be carefully chosen: The solution of the linearized problem of the mixing layer flow must be previously known to select appropriate wave numbers that lead to coherent structures and also the amplification rate of the perturbation. The effects of the gas/particles coupling as well as the gas compressibility are investigated. The range of convective Mach number considered is limited from 0.1 to 0.5. The linear stability results showed that, for higher convective Mach number, the two-dimensional perturbations become stable. Consequently, three-dimensional computations are needed to investigate flows with higher Mach number, which is beyond the scope of this study. The length scale and timescale of the vortex development, the evolution of the momentum thickness of the mixing layer, and the modal kinetic energy of the instability are also examined in this study.

Governing Equations

The analysis of the nonlinear development of a particle-laden mixing layer requires the numerical solution of the continuity, momentum, and energy equations of the particle and gas phases. The particle phase (dispersed phase) is assumed to be a continuum media. The volume fraction of the dispersed phase is supposed to be low enough to be considered a dilute flow. Thus, the volume fraction effects are neligible[13]: No pressure term arises in the dispersed-phase equations and information in this phase travels via the trajectories.[14] The gas phase is supposed to be compressible and inviscid: This assumption is physically justified by the inviscid nature of the Kelvin–Helmoltz instability.

The last assumption in such two-phase flows also means that the dissipative effects in the gas phase (due to the viscosity and the thermal conductivity) can be neglected in front of the interphasic effects (drag force, heat exchange). Thus, the flow is considered perfect except around particles. Nevertheless, the drag force depends on the gas viscosity, and the convective heat exchange depends on the thermal conductivity.

The principles of conservation of mass, momentum, and energy are applied and yield a system of partial differential equations describing the dynamics of both phases. The assumption of dilute two-phase flow implies that the gas and the dispersed phase equations are only coupled by source terms related to the interphasic exchanges. The source terms are in the right-hand side of the equations.

Gas phase:

$$\frac{\partial \rho}{\partial t} + \nabla \cdot \rho \boldsymbol{u} = 0 \tag{1}$$

$$\frac{\partial \rho \boldsymbol{u}}{\partial t} + \nabla \cdot (\rho \boldsymbol{u}\boldsymbol{u} + P\bar{\bar{I}}_d) = -\boldsymbol{F} \tag{2}$$

$$\frac{\partial \rho E}{\partial t} + \nabla \cdot \rho \boldsymbol{u}\left(E + \frac{P}{\rho}\right) = -\boldsymbol{F} \cdot \boldsymbol{u}_p - Q \tag{3}$$

Dispersed phase:

$$\frac{\partial \rho_p}{\partial t} + \nabla \cdot \rho_p \boldsymbol{u}_p = 0 \tag{4}$$

$$\frac{\partial \rho_p \boldsymbol{u}_p}{\partial t} + \nabla \cdot \rho_p \boldsymbol{u}_p \boldsymbol{u}_p = \boldsymbol{F} \tag{5}$$

$$\frac{\partial \rho_p E_p}{\partial t} + \nabla \cdot \rho_p \boldsymbol{u}_p E_p = Q + \boldsymbol{F} \cdot \boldsymbol{u}_p \tag{6}$$

with $E = C\nu T + \frac{1}{2}\boldsymbol{u}^2$ and $E_p = Cp_p T_p + \frac{1}{2}\boldsymbol{u}_p^2$. Cp_p is the heat capacity of the particles. The density of the dispersed phase ρ_p is expressed with the number of particle per unit volume n_p and the particle diameter d_p via the relation

$$\rho_p = n_p \rho_s \tfrac{1}{6}\pi d_p^3 \tag{7}$$

with ρ_s, the material density of the particle, supposed to be constant. (The particles are supposed to be spherical.)

A closure relation of the system of partial differential equations is given by the equation of state of the gas:

$$P = \rho R T \tag{8}$$

The source terms of Eqs. (1–6) represent the transfer between both phases. The Stokes law gives the drag force $\boldsymbol{F}$, and a correction is used through the C_d coefficient to take into account the deviation with the Stokes conditions:

$$\boldsymbol{F} = \rho_p C_d (\boldsymbol{u} - \boldsymbol{u}_p)/\tau_d \tag{9}$$

where τ_d is the dynamic relaxation time given by the relation

$$\tau_d = \rho_s d_p^{*^2} \big/ 18\mu \tag{10}$$

with μ the dynamic viscosity of the gas. The drag coefficient C_d is connected to the particle Reynolds number Re_p (Ref. 15),

$$C_d = 1 + 0.15 Re_p^{0.687} \tag{11}$$

The heat transfer Q is given by the following relation:

$$Q = \rho_p (Nu/2) Cp_p [(T - T_p)/\tau_t] \tag{12}$$

with $\tau_t = \rho_s Cp_p d_p^2 / 12\kappa_t$ the thermal relaxation time. The Nusselt number is given by an empirical relation[16]

$$Nu = 2 + 0.6 Re_p^{\frac{1}{2}} Pr^{\frac{1}{3}} \tag{13}$$

Some useful dimensionless parameters are defined to characterize the two-phase flow and to carry out a general analysis. The Stokes number $\mathrm{St} = \tau_d/\tau_f$ compares the dynamic relaxation time of the particles τ_d and the flow characteristic time τ_f. The latter will be defined next.

The global mass loading ratio is an important parameter that will be largely used to characterize the two-phase flow. This ratio is the total mass of particles to the total mass of the gas in the initial flow:

$$Z = \frac{m_p}{m_g} = \frac{\rho_s V_p}{\rho V_g} = \frac{\rho_s n_p \left(\pi d_p^3 \big/ 6\right) V_T}{\rho V_g}$$

V_k is the total volume of the phase k. The total volume of the mixture is defined by $V_T = V_p + V_g$. Because the volume fraction is very low in the case of dilute flow, leading to $V_T \approx V_g$, the expression of Z is then reduced to

$$Z \approx \rho_s n_p \left(\pi d_p^3 / 6\right) / \rho \approx \rho_p / \rho \tag{14}$$

It is generally admitted that the volume fraction of the dispersed phase α_p must be bounded by $\alpha_p \leq 10^{-2}$ for dilute flows. One can write $Z = \alpha_p \rho_s / \rho$. This relation shows that the order of magnitude of Z must not exceed 10 to verify the dilute flow assumptions if we consider $\rho_s / \rho \approx 10^3$ as a typical value for gas/particles mixture. In the following, Z will refer to the initial mass loading ratio, which is fixed for a simulation on the contrary to the local densities ratio ρ_p / ρ.

This system of equations is then numerically solved to simulate the behavior of a two-dimensional particle-laden compressible mixing layer. Appropriate initial conditions are required, based on the analysis of the linear development of this flow.[12]

Numerical Issue

Numerical Scheme

The partial differential equations (1–6) are written in the general conservative form

$$\frac{\partial U_g}{\partial t} + \nabla \cdot \boldsymbol{F}(U_g) = \boldsymbol{H}_g(U_g, U_p)$$

$$\frac{\partial U_p}{\partial t} + \nabla \cdot \boldsymbol{F}(U_p) = \boldsymbol{H}_p(U_g, U_p) = -\boldsymbol{H}_g(U_g, U_p)$$

with $U_g = (\rho, \rho \boldsymbol{u}, \rho E)^T$ and $U_p = (\rho_p, \rho_p \boldsymbol{u}_p, \rho_p E_p)^T$. The flux vectors $\boldsymbol{F}(U_k)$ are directly deduced from Eqs. (1–6), and the vector $\boldsymbol{H}$ contains the source terms related to the different transfers.

The same second-order in space and time, finite volume scheme is used to solve both systems of equations. This scheme is based on a MUSCL method, a second-order extension of Godunov's method. The use of this method is justified by previous works of Lumpp and Guillard[17]: The ability of the method to simulate sigle-phase compressible mixing layers with subsonic convective Mach numbers was proven. The accuracy obtained on a computation grid of 101×101 cells is of the same order compared to the results given by a spectral method.[18] Higher grid resolution is needed for transonic convective Mach number when shock waves appear during the mixing layer development, but these cases will not be investigated in the present study.

An operator splitting is used to compute the solution according the sequence $U_k^{n+1} = L_{\text{sour}} L_{\text{conv}}(U_k^n)$. The two operators are defined by

$$\tilde{U}_k = L_{\text{conv}}\left(U_k^n\right)$$

with $\tilde{U}_k$ the solution of

$$\frac{\partial U_k}{\partial t} + \nabla \cdot \boldsymbol{F}(U_k) = 0, \qquad U_k^{n+1} = L_{\text{sour}}(\tilde{U}_k)$$

with U_k^{n+1} the solution of

$$\frac{\mathrm{d}U_k}{\mathrm{d}t} = \boldsymbol{H}_k$$

where L_{conv} is the finite volume scheme used to solve the conservative equations. The flux vectors $\boldsymbol{F}$ are computed by means of exact Riemann solvers for both phases. The L_{sour} operator is the integration of the interaction terms and is defined by a fourth-order Runge–Kutta scheme. The complete method is detailed by Thevand et al.[19] and Thevand[20] with numerous validation cases. These test cases include one-phase flow validations (propagation of shock waves and boundary-layer developments) as well as two-phase flows (two-phase flows, boundary layers, shock waves, acoustic waves propagation, and nozzle flows).

A diffusion term has to be included in the dispersed-phase conservation equations due to numerical considerations as proposed by Wang et al.,[10] who considered this term as a first-order model for particle momentum diffusion due to local particle/particle interactions,[21]

$$\frac{\partial U_p}{\partial t} + \nabla \cdot \boldsymbol{F}(U_p) - \kappa \nabla^2 U_p = \boldsymbol{H}_p \tag{15}$$

This term removes small-scale singularities generated by local high particle concentration spots and is vanishing for smooth solutions. The value of the diffusion coefficient is related to the timescale and length scale as well as local flow and particles characteristics. The following relation is used in the simulations that will be discussed here:

$$\kappa = 2 \times 10^{-3} u \delta \tag{16}$$

where u is a characteristic velocity and δ a characteristic length. Their value will be given in the next section. The constant value was carefully chosen to not change the flow characteristics except for the singularities: Qualitative comparisons on isovalues were done, as well as comparisons on quantities that integrate two-phase effects over the simulations, like the momentum thickness and the modal energy distribution.

Mesh Sizing and Boundary Conditions

The computations are performed on a 128×128 mesh. The mesh size is $Lx = 2\lambda_f$ in the streamwise direction and $Ly = 3\lambda_f$ in the transverse direction, where λ_f is the fundamental wavelength of the perturbation, $\lambda = 2\pi/\alpha$. The size is given by preliminary linear studies of the system of equations. The gird spacing is uniform in the x direction and stretched in the y direction.

The computational domain is periodic in the x-coordinate direction, which leads to the numerical condition

$$U|_{x=0} = U|_{x=Lx} \tag{17}$$

In the y-coordinate direction, nonreflecting boundary conditions are determined for the gas phase to replace the left wave (subsonic flow), whereas an extrapolation of the conservative variables is computed for the dispersed phase.

Initial Conditions

The mixing layer considered in this investigation is composed of two parallel streams laden with spherical solid particles. The subscripts 1 and 2 refer to the upper and lower freestream conditions of the flow, respectively. The streamwise and transverse coordinates are denoted by x and y, respectively. The equations are nondimensionalized with reference variables from the upper side of the layer: u_1, ρ_1, P_1, and T_1. The length scale is chosen to be the initial vorticity thickness δ_0 (Fig. 1):

$$\delta_0 = (u_1 - u_2) \Big/ \left(\frac{\mathrm{d}u}{\mathrm{d}y}\right)_{y=0} \tag{18}$$

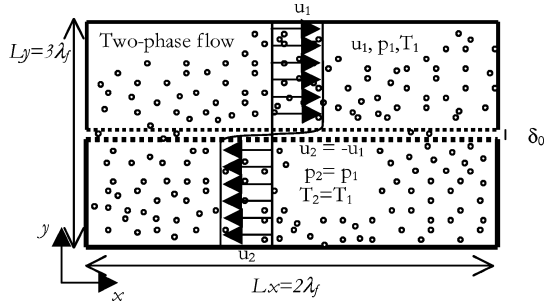

Fig. 1 Schematic view of the two-phase mixing flow.

where $y=0$ is the initial position of the interface between both streams. The flow characteristic time can now be defined by $\tau_f = \delta_0/u_1$.

The initial conditions of the flow are obtained by a preliminary analysis of the linearized equations, which requires the decomposition of the physical variables into their mean and fluctuating parts denoted $\bar{f}$ and $\tilde{f}$, respectively,

$$f = \bar{f} + \tilde{f} \tag{19}$$

The fluctuating components of the initial physical variables are modeled with the general form of two-dimensional traveling waves:

$$\tilde{f} = \varepsilon_0 \hat{f}(y) e^{i(\alpha x - \omega i)} \tag{20}$$

where ε_0 is the initial amplitude of the disturbance, $\hat{f}$ is a complex eigenfunction dependent only on the flow coordinate y, α is the wave number in the streamwise direction, and ω is the disturbance frequency. For the temporal stability analysis, α is real and ω is complex. The imaginary part of ω, denoted ω_i, is the amplification rate of the perturbation. The disturbance characteristics used as the initial values in this study correspond to the most amplified disturbance and its first subharmonic mode. These characteristics, $\omega_{i,\max}$, α, and $\hat{f}(y)$ are obtained by solving the linear system of equations derived from Eqs. (1–6) (Ref. 12).

When the mean quantities are considered, the velocities of the streams are supposed to be equal and opposite, which leads to a velocity profile of the gas phase of the form $\bar{u}(y) = u_1 \mathrm{erf}[\sqrt{(\pi)}y]$. The gas pressure and temperature are assumed to be constant throughout the mixing layer. The initial mean flow is characterized by a thermal and dynamic equilibrium between both phases, yielding $\bar{T}_p = \bar{T}$ and $\bar{u}_p = \bar{u}$. In this study, particles are uniformly distributed in the flow. This work could be extended to nonuniform density distribution as it was done by Wen and Evans,[22] who studied the effects of nonuniform particle loading in the incompressible mixing layer. These authors report the development of secondary instability modes. The existence of such instability should be checked for compressible flows, but this is beyond of the focus of this study.

Results

Introduction

Numerous studies have shown that the compressibility has an important stabilization effect on the perturbation development in a single-phase flow.[23–28] The compressibility is usually characterized by the convective Mach number, that is, $M_c = (u_1 - u_2)/(a_1 + a_2)$ (In the present conditions, $a_1 = a_2$.) The initial mass loading ratio Z is also an important parameter to characterize the two-phase flow. The simulations presented here are restricted to $Z=0$ (one-phase flow) and $Z=1$. Indeed, some regions of the flow (braids) may present local accumulations of particles leading to large values of the local density ratio ρ_p/ρ. An initial value $Z=1$ maintains, during the unsteady calculations, a maximal order of magnitude of $\rho_p/\rho \approx 10$. Thus, the dilute flow assumption remains valid. The two-phase flow is also characterized by the ratio of the heat capacities $Cp_p/Cp = 1.21$, $\rho_s = 1700$ kg/m^3, and $Pr = 0.7$.

Linear Results

First, the main results of the linear analysis obtained in a previous work[12] are recalled to clarify the present study.

The flow perturbation is characterized by the maximum amplification rate $\omega_{i\max}$. It corresponds to the values of the wave number α that will generate a disturbance preferentially amplified by the flow. In Fig. 2, $\omega_{i\max}$ vs the convective Mach number is shown for typical values of $\alpha\mathrm{St} = \tau_d/\tau_{\mathrm{peri}}$ product, which appeared to be a more pertinent parameter than the Stokes number generally used. (Here τ_{peri} is a characteristic time of the perturbation based on the wave number.) The values of αSt are set to 0.1, 1, and 10, which correspond to small, intermediate, and large particle inertia, respectively when compared with the perturbation characteristic time of the fundamental mode. Particles have an important influence on

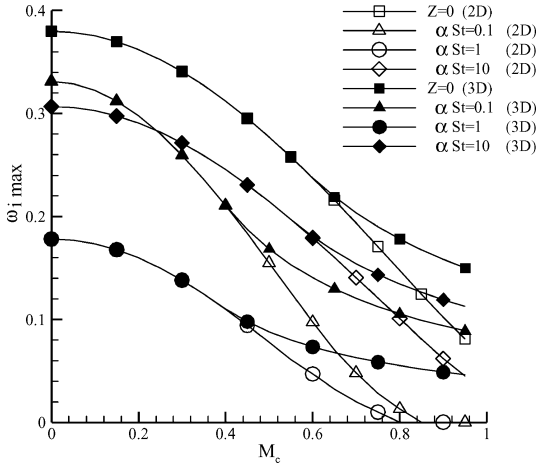

Fig. 2 Linear instability growth rate vs the convective Mach number.

the obliquity angle of the most amplified perturbation. This perturbation remains two dimensional up to a convective Mach number $M_c \approx 0.35$ then becomes three dimensional for higher Mach number values. The influence of the particles on this transition is maximum for low or average particle inertia. In Fig. 2, the filled symbols correspond to three-dimensional linear calculations, which means that the most amplified disturbance is sought by varying the obliquity angle of the initial perturbation. (This disturbance can be either two or three dimensional.) The empty symbols correspond to calculations achieved for two-dimensional disturbances. This comparison between two- and three-dimensional linear calculations justify that two-dimensional nonlinear computations are performed for convective Mach number less than 0.5. Indeed, this study has not been extended to flows with larger Mach number because $\omega_{i\max}$ tends rapidly to zero for two-dimensional perturbations. Also notice in Fig. 2 that whatever the case, $\omega_{i\max}$ is lower when particles are present in the flow than for a single-phase flow ($Z=0$): In an inviscid flow, inert particles always have a stabilization effect on the perturbation. The minimum value is obtained for $\alpha\mathrm{St} \sim 1$, whatever the convective Mach number. Particles with low inertia ($\alpha\mathrm{St} = 0.1$) tend to follow the gas fluctuations, whereas for particles with large inertia ($\alpha\mathrm{St} = 10$) the dynamics of the gas and the particles are less dependant than for $\alpha\mathrm{St} \sim 1$. The value of $\omega_{i\max}$ decreases when the convective Mach number is increased. The stabilization effect of the compressibility is added to the dispersed-phase inertia effect. Notice that compressibility and particle inertia effects are dependent: The stabilization effect of the particles is stronger for $\alpha\mathrm{St} = 10$ than for $\alpha\mathrm{St} = 0.1$ when compressibility effects are low ($M_c \sim 0$), but this tendency is reversed when the convective Mach number of the flow is increased.

Nonlinear Development

For the nonlinear study, the product αSt is still used as a main parameter for the analysis. Only two-dimensional flows are considered for subsonic Mach numbers varying in the range $M_c = 0.1$–0.5. The most amplified perturbation in particle-laden flows is theoretically three dimensional for $M_c = 0.5$, but it is interesting to study the coupling of compressibility and particle effects on the two-dimensional flow structures when the convective Mach number is increased.

The flow is initially perturbed on the fundamental, α_f, and first subharmonic, $\alpha_s = \alpha_f/2$, modes of the most amplified two-dimensional perturbation. The wave numbers, the growth rates, and the eigenfunctions of these perturbations are given by the linear analysis. The fundamental mode wave numbers and growth rates are given in Table 1 for a single-phase flow and gas/particle flows with $Z=1$. The amplitude of the perturbation is fixed equal to $\varepsilon_0 = 8 \times 10^{-3}$ and 2×10^{-3} for fundamental and the subharmonic modes, respectively.

Figure 3 shows the evolution of the gas vorticity fields during the mixing layer development for low-compressibility effects

($M_c = 0.1$). These results are given for a single-phase flow, $Z = 0$, and particle-laden flows with a constant mass loading $Z = 1$. The $\alpha_f \mathrm{St}$ product varies from $\alpha_f \mathrm{St} = 0.1$ (small inertia particles) to $\alpha_f \mathrm{St} = 10$ (large inertia particles). The vorticity fields are shown at four representative times in the flow evolution. The results at the second and the fourth time show the rollup of the voriticity sheet and the subsequent pairing of neighbouring vortices, respectively. The time of these events depends on the amplification rate of the perturbation. In general, Fig. 3 shows that typical sequences of the mixing layer development are still recovered for a compressible two-phase flow: the rollup of the vorticity sheet, the vortex formation, and the pairing of vortices. These results are qualitatively close to the Wang et al.[10] results for an incompressible particle-laden flow with a finite Reynolds number ($Re = 250$). The shapes of the vortices obtained for the different particle inertia are similar. In the present study, the Reynolds number is infinite, and consequently, no quantitative comparisons with the Wang et al. results can be performed, even when compressibility effects are weak.

Table 1 Fundamental mode characteristics ($Z = 1$, except for one phase $Z = 0$)

Flow characteristic	$M_c = 0.1$		$M_c = 0.35$		$M_c = 0.5$	
	α_f	ω_{if}	α_f	ω_{if}	α_f	ω_{if}
One phase	0.86	0.37	0.80	0.33	0.74	0.28
$\alpha_f \mathrm{St} = 0.1$	0.80	0.32	0.68	0.24	0.52	0.15
$\alpha_f \mathrm{St} = 1$	0.54	0.17	0.46	0.13	0.36	0.08
$\alpha_f \mathrm{St} = 10$	0.74	0.30	0.70	0.26	0.66	0.22

In this unstable configuration, the gas naturally rolls up, whereas the particles will naturally tend to flow in the streamwise direction. The drag force will perturb this motion: For small particle inertia ($\alpha_f \mathrm{St} = 0.1$), the particles tend to follow the fluid motion, thus, the momentum exchange is low. The evolution of the gas vorticity field is globally close to the single-phase flow evolution. If the particle inertia is increased up to $\alpha_f \mathrm{St} = 1$, the particles will tend to go to the periphery of the vortex, and a part of the gas vorticity will be distributed in the steamwise direction. There is a large exchange of momentum because of higher particle density at the periphery. This tendency is reversed for $\alpha_f \mathrm{St} > 1$, due to the decrease of the drag effects. A calculation (not given here) with $\alpha_f \mathrm{St} = 100$ shows that the gas behavior is no longer affected by the particles and single-phase flow results are recovered: The particle inertia is so large, the dispersed phase cannot affect the gas phase, the dynamic relaxation time being much larger than the timescale of the perturbation.

Notice a rupture of the vortical structure, which appears as a low vorticity layer in the region near the vortex periphery (clear area). Wang et al.[10] explained this rupture as the removal of local fluid

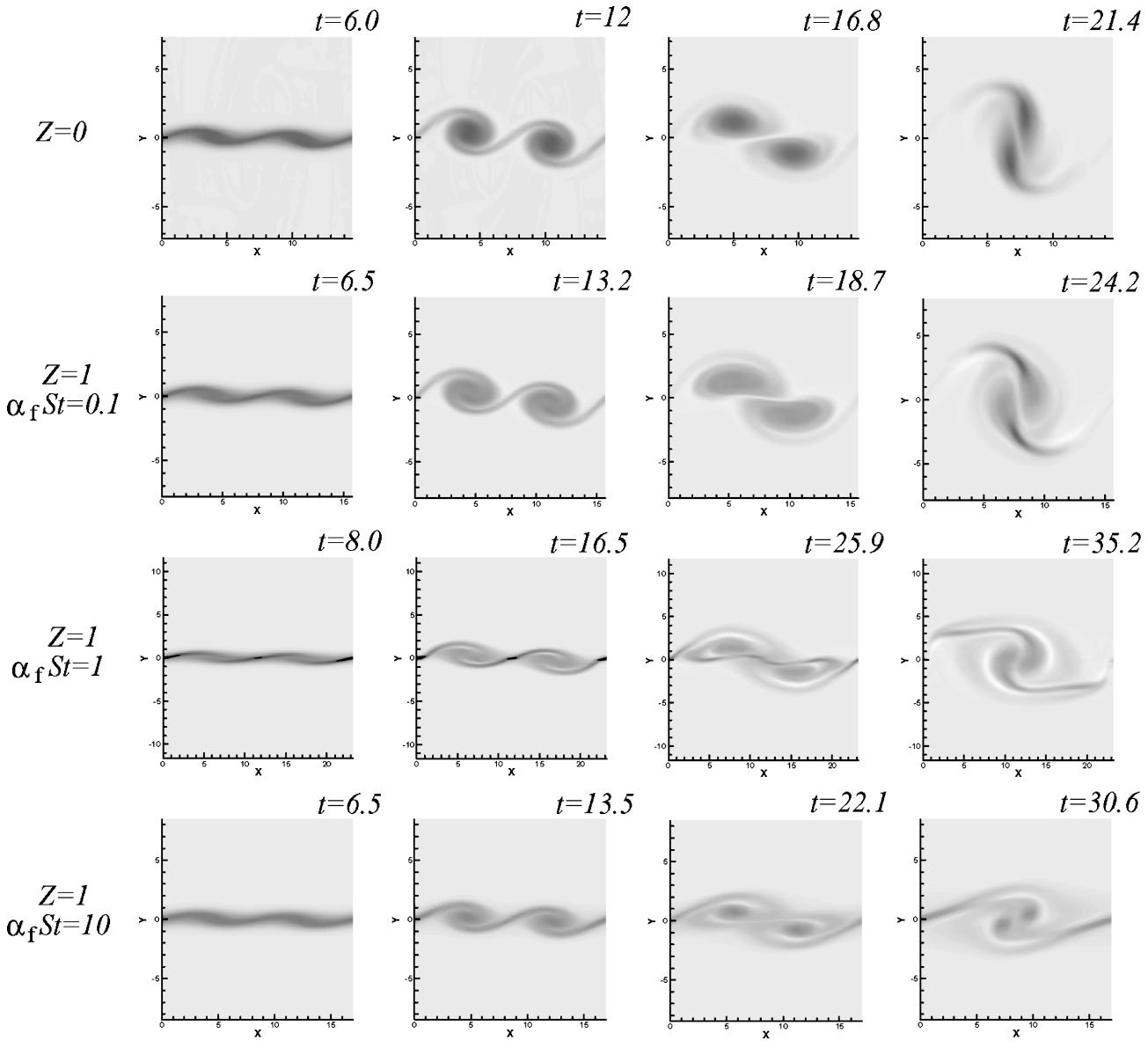

Fig. 3 Gas vorticity field for $M_c = 0.1$; maximum = 220 (black) and minimum = −20 (white).

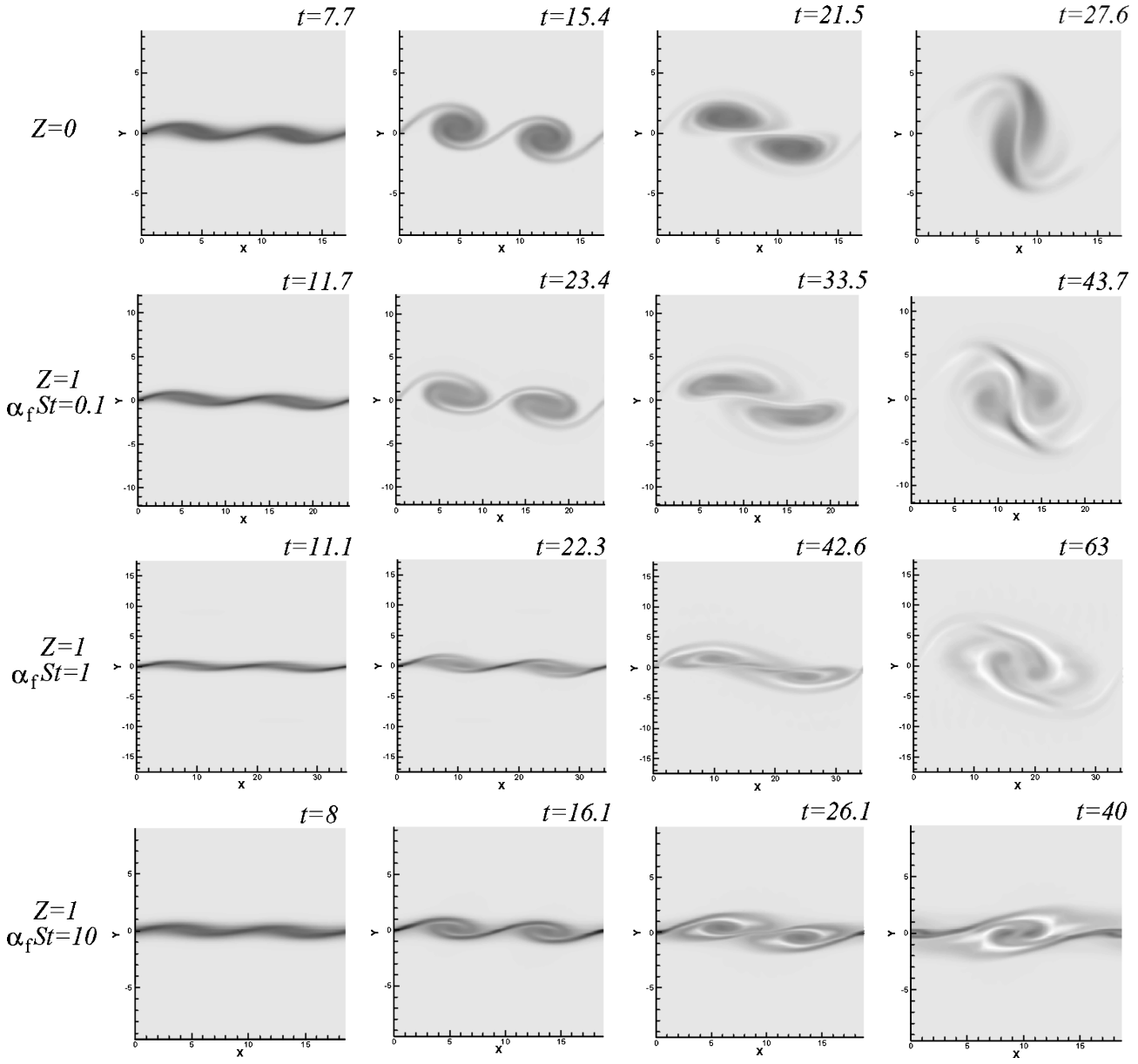

Fig. 4 Gas vorticity field for $M_c = 0.5$; maximum = 900 (black) and minimum = −100 (white).

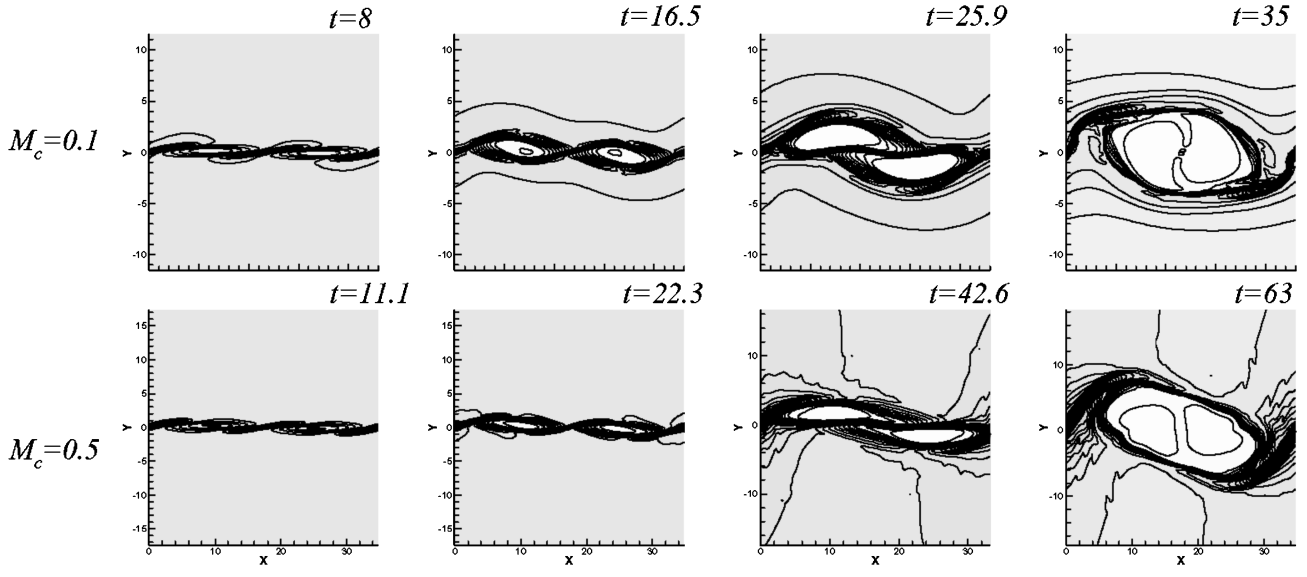

Fig. 5 Particle density distribution for $\alpha_f \mathrm{St} = 1$; maximum = 30 (black) and minimum = 0 (white).

vorticity by the particles that play the role of vorticity sink. This explanation does not seem to be general: At the braids between the vortices, a high particle concentration is generally observed, which now creates vorticity. The vorticity field characteristics are dependent on the case, as well as the time considered:

1) During the rollup, the results show a displacement of the vorticity from the center to the periphery of the vortex when $\alpha_f \mathrm{St}$ is increased. When the dynamic coupling between both phases is maximal ($\alpha_f \mathrm{St} = 1$), the whole vorticity is concentrated at the braids between the two initial vortices in a very thin layer. For larger $\alpha_f \mathrm{St}$, the vorticity goes back to the center at this specific time step.

2) At the pairing time, observe that vorticity peaks are located in the center of the final vortical structure for single-phase and low inertia particle-laden flows. When $\alpha_f \mathrm{St}$ is close to 10, an important part of the vorticity is depleted to the braids between the final structures (corresponding to the periodic limits of the computation domain). This vorticity goes back to the center when $\alpha_f \mathrm{St}$ is increased. For very large $\alpha_f \mathrm{St}$, the vorticy field is quite similar as the one-phase flow solution ($\alpha_f \mathrm{St} = 100$, not shown here).

We can conclude that the presence of larger particle concentration involves a large drag effect that locally creates or removes vorticity in the gas phase. According the present results, one cannot guess the prevalence of one or the other behavior.

The addition of particles in the flows stretches the shape of the vortices. This is due to initial length scale of the perturbation. The size of the first formed vortices corresponds to the fundamental wavelength. Thus, the streamwise length scale of the vortices increases when the mode of the initial perturbation is shifted to smaller wave number. Refer to Table 1: Note that the wave number is minimum for $\alpha f \mathrm{St} = 1$, which leads to the most important length scale of the vortical structures shown in Fig. 3. In this case, the size of the structure in the x direction at the vortex coupling time, $t = 35.2$, is 1.6 times more important than for a single-phase flow, $t = 21.4$. This leads to a stretched shape of the vortices because the order of magnitude of the length scale in the y direction remains roughly the same in single- and two-phase flows: The aspect ratio is not conserved. Moreover, note a small decrease of the vortex length scale in the y direction for $\alpha_f \mathrm{St} = 10$ at the pairing time.

When the timescale of the flow evolution is considered, it is obviously more important when particles are present in the flow: The time development of the vortical structure depends on the linear growth rate of the perturbation, which is lower when two-phase flows are considered (Table 1).

The convective Mach number of the flow is now increased and equal to 0.5. In Fig. 4, the temporal evolution of the gas vorticity is plotted for single-phase and two-phase ($Z = 1$) flows.

For the single-phase flow, the gas vorticity field evolution is qualitatively close to the one obtained for $M_c = 0.1$, although the regions of high vorticity appear more diffused when the convective Mach number increases. The time development is obviously different because the growth rate depends on the Mach number (Table 1).

The structures of the particle-laden flow are more influenced by the compressibility effects than the single-phase flows. The vortices formed during the rollup of the initial vortex sheet are more elongated, especially for low, $\alpha_f \mathrm{St} = 0.1$, and intermediate, $\alpha_f \mathrm{St} = 1$, particle inertia. In these cases, the length scale in the y direction increases by comparison with the results obtained at $M_c = 0.1$. Note that for particle-laden flows with $\alpha_f \mathrm{St} = 10$ the structure resulting from the vortex pairing, $t = 32$, is very compact. The decrease of the length scale in the y direction for $\alpha_f \mathrm{St} = 10$ is more important than for $M_c = 0.1$, and the radial length of the vortical structure reaches the half that obtained for a single-phase flow.

A comparison of the particle density evolution between $M_c = 0.1$ and $M_c = 0.5$ ($\alpha_f \mathrm{St} = 1$) can be seen in Fig. 5. The changes in the gas vorticity field when the convective Mach number is increased lead to a different distribution of the particle density. The particle density fields are shown at the four times introduced earlier. The clear zones in Fig. 5 correspond to particle-free areas, whereas the dark areas represent local high particle density zones, upto $\rho_p/\rho \approx 10$. For $\alpha_f \mathrm{St} = 1$, the particles are centrifuged from the core of the vortices and accumulate at the periphery of the coherent structures. This migration of the particles during the flow evolution is obtained for $M_c = 0.1$ and 0.5. The results of two-phase flow characterized by a smaller or larger particle inertia are not shown. For $\alpha_f \mathrm{St} = 0.1$, the particles follow the fluid motion. There is no particle-free zone in this case, and the particle density scales from 0.1 to 1. The distribution of the particle in the flow is little affected when the Mach number is increased. For $\alpha_f \mathrm{St} = 10$, the particles disperse at low rates. The results show the particle migration toward the periphery of the vortices, but the particle density variations and the magnitude of low particle density areas are less important than for $\alpha_f \mathrm{St} = 1$.

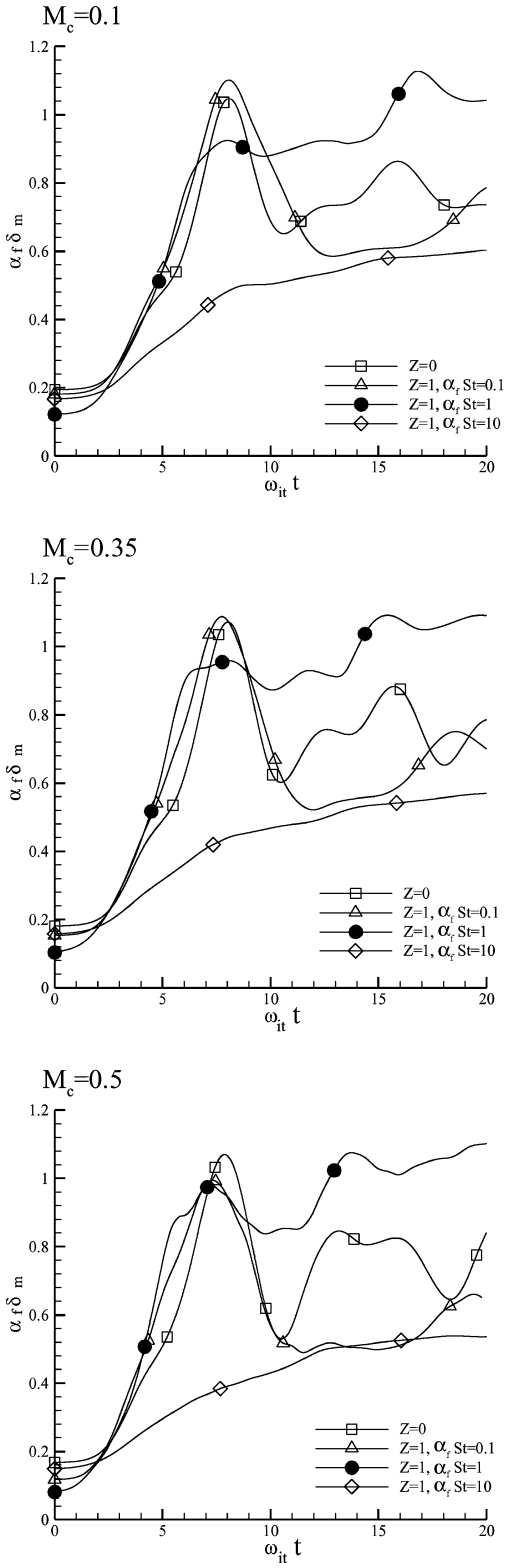

Fig. 6 Momentum thickness vs time.

Momentum Thickness

Figure 6 shows a comparison of the temporal evolution of the mixing layer momentum thickness δ_m for different convective Mach number, $M_c = 0.1$, 0.35, and 0.5, and for different $\alpha_f \mathrm{St}$ numbers. The momentum thickness, calculated with horizontal averaged quantities, is normalized by α_f, and the time is normalized by ω_{if}. In Fig. 6, one can directly compare the one-phase and the two-phase solutions. Indeed, notice that the typical flow development stages occur roughly at the same normalized time and that the time evolution is qualitatively the same whatever the Mach number considered. The first peak obtained for single-phase flows ($Z = 0$) and particle-laden flows ($Z = 1$) with $\alpha_f \mathrm{St} = 0.1$ corresponds to the vortex pairing time ($\omega_{if} t \approx 8$). For $\alpha_f \mathrm{St} = 1$ and 10, the vortex pairing time appears only as a change of the slope of δ_m (at $\omega_{if} t \approx 6$ for $\alpha_f \mathrm{St} = 1$ and $\omega_{if} t \approx 9$ for $\alpha_f \mathrm{St} = 10$). Note that the amplitude of the normalized momentum thickness for $\alpha_f \mathrm{St} = 0.1$ and 1 at this specific time remains relatively close to the single-phase flow amplitude, contrary to the results obtained for $\alpha_f \mathrm{St} = 10$. This corresponds to

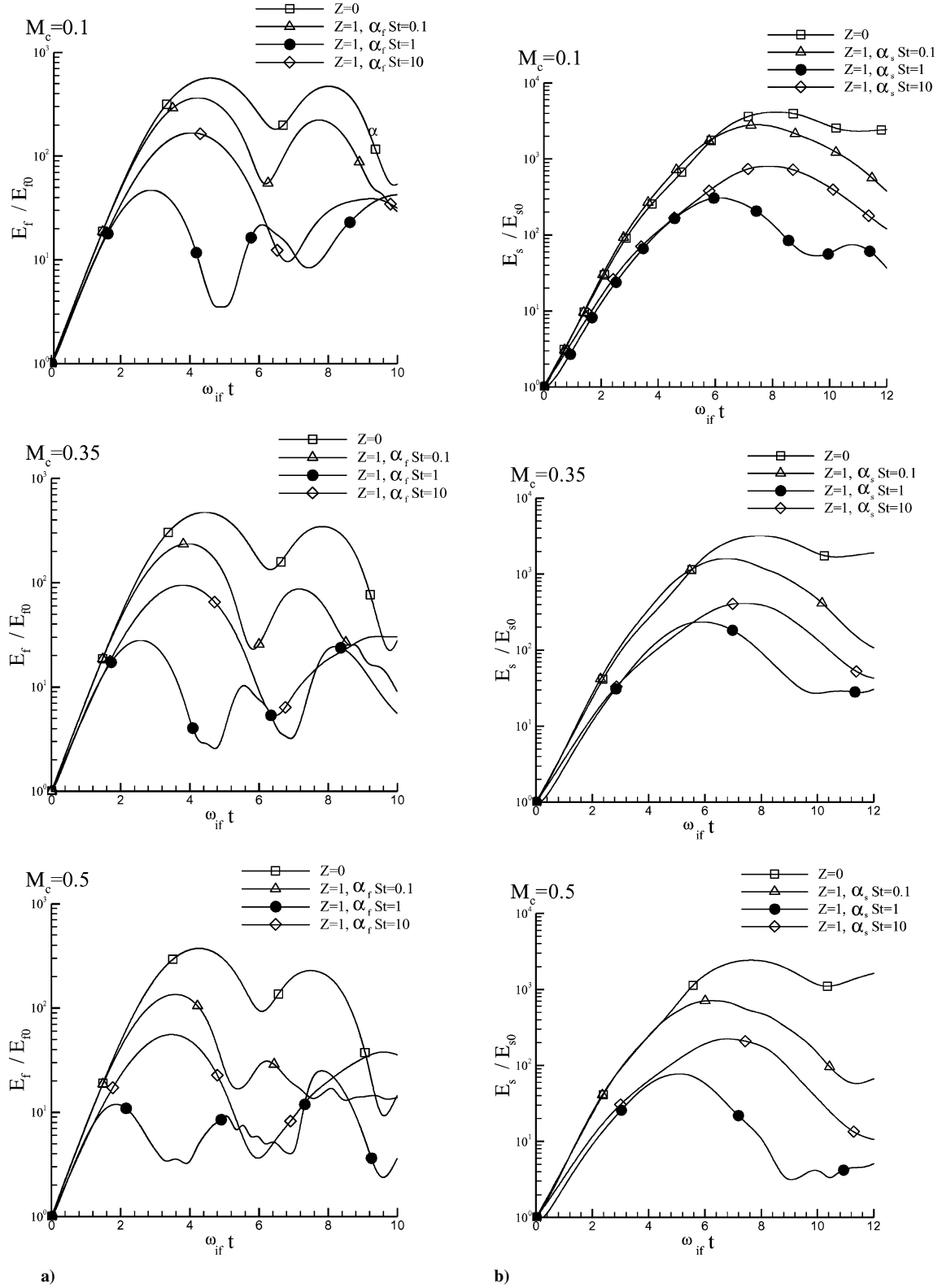

Fig. 7 Modal kinetic energy vs time: a) fundamental mode and b) first subharmonic mode.

the reduction of the transversal amplitude of the vortical structure by comparison with the streamwise length scale noticed earlier for $\alpha_f \mathrm{St} = 10$ (Figs. 3 and 4). For single-phase flows and particle-laden flows with $\alpha_f \mathrm{St} = 0.1$, the maximum amplitude of the momentum thickness is obtained with the first peak. The momentum thickness evolution is different for particle flows with intermediate and large inertia, $\alpha_f \mathrm{St} = 1$ and 10: The momentum thickness continues to grow after the vortex pairing time, and the mixing layer tends to grow more regularly. Even if the different evolutions are qualitatively similar, there are some slight differences when the Mach number is increased ($M_c = 0.5$). When particle-laden flows are considered, there is a small shift of the pairing time and a small decrease of the momentum thickness amplitude. Nevertheless, the effects of coupling between compressibility and particle inertia on the mixing layer development do not appear clearly in Fig. 6. The momentum thickness is a global quantity that reveals qualitative evolutions, and it is difficult to extract one specific effect in the nonlinear evolution of the mixing layer.

Modal Kinetic Energy

The temporal evolution of the gas kinetic evolution is now studied to point out the effects of the particles and those of the compressibility. In Fig. 7, the evolution of the gas kinetic energies of fundamental (Fig. 7a) and subharmonic (Fig. 7b) modes is plotted as a function of time. For each mode k, the kinetic energy is given by

$$e(k) = \frac{1}{Ly} \int_0^{Ly} [\hat{u}(k, y)]^2 + [\hat{v}(k, y)]^2 \, \mathrm{d}y \qquad (21)$$

where $\hat{u}(k, y)$ and $\hat{v}(k, y)$ are the Fourier transform of the gas velocity components. The energies are normalized by their initial values and the time by ω_{if}. The first part of each curve is linear and corresponds to the linear development of the instability. Then the fundamental and subharmonic fluid modal energies reach a peak. The first peak of the fundamental fluid modal energy corresponds to the rollup of the mixing layer and the formation of the first vortices, whereas the first peak of the subharmonic modal energy corresponds to the vortex pairing and the formation of larger coherent structures.

The effects of the coupling between the compressibility and the particle inertia can be observed by comparing the energy peak values between $M_c = 0.1$ and 0.5. There is a more important decrease of the fluid modal energies for particle-laden flows than for single-phase flows, when the convective Mach number is increased. This decrease is obtained for both fundamental and subharmonic modes.

A particular phenomenon is observed when particles are considered: The addition of particles accelerates the appearance of the first peak. This phenomenon is accentuated when the particle inertia is intermediate, $\alpha \mathrm{St} = 1$, showing a stronger coupling than for the other cases.

In Ref. 10, the Stokes number St is used as the particle inertia parameter, and the authors concluded there is a decrease of the peak magnitude of the fundamental and subharmonic fluid modal energy for increasing Stokes number. In the present study, the αSt product is chosen to characterize the particle inertia, leading to different conclusions. The peak magnitude of the fundamental and subharmonic fluid modal energy is much smaller for intermediate particle inertia, $\alpha_f \mathrm{St}$ and $\alpha_s \mathrm{St}$ of the order of unity, than for lower or larger values (reverse-bell shape). This result is more reasonable with the linear stability results, which have showed that for very high or very low particle inertia the two-phase coupling effects are lower than for intermediate particle inertia and vanish for asymptotic values of particle inertia.

For better accuracy, simulations for other αSt values are performed. The results are summarized in Fig. 8. Figure 8 shows the evolution of the first peak magnitude of the fundamental and subharmonic modal energies vs αSt. Note that the first peak of the fundamental fluid modal energy corresponds to the formation of the smaller vortices, whereas the first peak of the subharmonic modal energy corresponds to the formation of the larger coherent

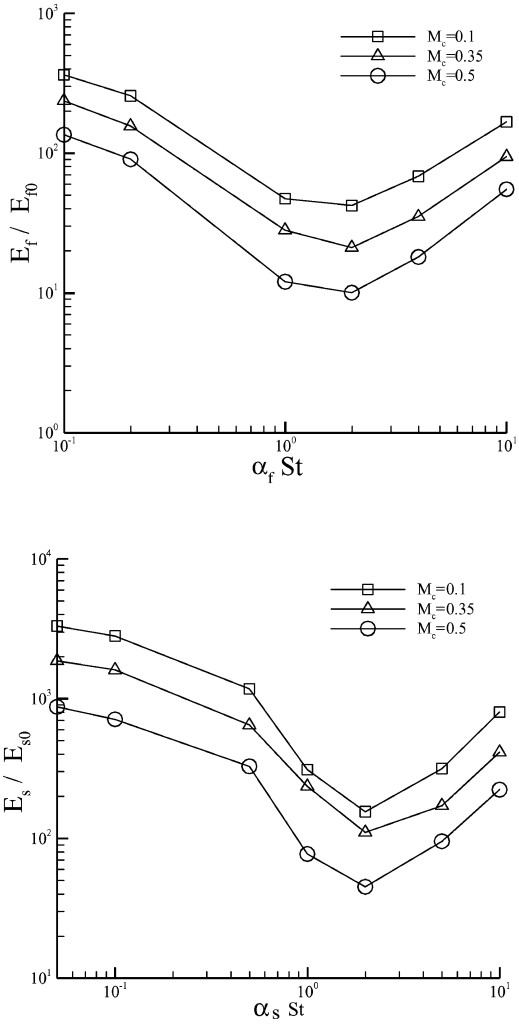

Fig. 8 Maximum modal energy vs particle inertia.

structures. As noticed earlier, the energy magnitude decreases when the convective Mach number is increased. Whatever the convective Mach number, the minimum magnitude of the fluid modal energy is reached for αSt of the order of 2 for the fundamental, as well as the subharmonic, mode. This similarity in the curves obtained for each mode is very interesting. This result shows that the nonlinear effects due to the vortex formation, the vortex pairing, and the consequent redistribution of the particle density in the mixing layer do not dramatically change the relation between the energy of vortical structures and the particle inertia parameter αSt. Indeed, the energy decrease obtained for the structures generated by the development of the fundamental mode is similar to the one obtained for the structures generated by the development of the subharmonic mode. Nevertheless, it also means that it is not an easy task to model the kinetic energy dissipation of the gas phase because of the presence of particles. For example, a linear relation with the Stokes number would have led to a simple result, but this nonlinear behavior, summarized in Fig. 8, prevents a simple relation from being obtained. The energy dissipation is maximal for αSt around unity, showing a nonlinear coupling between the energy dissipation, the wavelength of the perturbation, and the Stokes number. This point is very important when modeling such an energy transfer.

We have restricted our investigations to the development of two harmonic modes, but we could extend this result and make the assumption that, for a vortical structure with a given length scale, the vortex energy damping generated by two-way coupling is more important when the particle relaxation time is of the order of the specific development time of this coherent structure. This assumption has to be verified by further investigation.

Conclusions

The nonlinear development of a two-phase dilute compressible mixing layer has been conducted for low Mach number. Limited works are devoted to this topic, and the present work is an original one, in which two-phase effects (and its associated two-way coupling) and compressibility are considered. In this range of Mach number, the use of a finite volume scheme was proven efficient by other published works, and it is successfully extended for two-phase flows. The use of an Eulerian approach for the description of particle phase is also suitable for such calculations. The linear development of the mixing layer is well computed, and results can be compared with some obtained with use of a Lagrangian approach.

This numerical study shows the important influence of two-way coupling on the dilute particle-laden compressible mixing layer. This influence, depending on the particle inertia parameter $\alpha \mathrm{St}$, leads to important changes in the shape and the main characteristics of the vortical structures. For intermediate particle inertia, the vortices are more elongated, and the study of the momentum thickness shows that the mixing layer tends to grow more regularly. The effects are maximal for $\alpha \mathrm{St} = 1$, that is, when the coupling between the dynamics of the particles and the instability is the highest.

In the range of the Mach number investigated, the particle-laden mixing layer is more influenced by the compressibility effects than the single-phase flow. This influence is visible in the shape of the vortical structures, which are stretched for particle-laden flows when the convective Mach number increases. The results also show a more important decrease of the fluid modal energy for particle-laden flows, suggesting that the compressibility effects amplify the dissipation of the vortex kinetic energy by the momentum exchange between the gas and the particles.

The magnitude of the fluid modal energy of both the fundamental and subharmonic modes is found to be a minimum for all convective Mach numbers investigated, at $\alpha \mathrm{St} \approx 2$. The reason for this very specific value is not obvious because one would have expected it at $\alpha \mathrm{St} \approx 1$ because the coupling is maximal for this value. Nevertheless, this result suggests that the two-way coupling effects on a coherent structure remain more important when the particle relaxation time is of the order of the specific development time of this structure. The particle density redistribution due to the previous development of the harmonic mode has little impact on this relation. This result shows that a study of the coupling between the dispersed-phase behavior and the instability cannot be carried out only with the Stokes number. This number should be directly compared to the characteristic time of the perturbation.

References

[1]Saffman, P. J., "On the Stability of Laminar Flow of a Dusty Gas," *Journal of Fluid Mechanics*, Vol. 13, 1962, pp. 120–128.

[2]Michael, D. H., "Kelvin–Helmholtz Instability of a Dusty Gas," *Proceedings of the Cambridge Philosophical, Society*, Vol. 61, 1965, pp. 569–571.

[3]Tong, X. L., and Wang, L. P., "Two-Way Coupled Particle-Laden Mixing Layer. Part 1: Linear Instability," *International Journal of Multiphase Flow*, Vol. 25, No. 4, 1999, pp. 575–598.

[4]Yang, Y. Q., Chung, J. N., Troutt, T. R., and Crowe, C. T., "The Influence of Particles on the Spatial Stability of Two-Phase Mixing Layers," *Physics of Fluids*, Vol. 2, 1990, pp. 1839–1845.

[5]Lazaro, B. J., and Lasheras, J. C., "Particle Dispersion in the Developing Free Shear Layer, Part I: Unforced Flow," *Journal of Fluid Mechanics*, Vol. 235, 1992, pp. 143–178.

[6]Lazaro, B. J., and Lasheras, J. C., "Particle Dispersion in the Developing Free Shear Layer, Part II: Forced Flow," *Journal of Fluid Mechanics*, Vol. 235, 1992, pp. 179–221.

[7]Wen, F., Kamalu, N., Chung, J. N., Crowe, C. T., and Troutt, T. R., "Particle Dispersion by Vortex Structures in Plane Mixing Layers," *Journal of Fluids Engineering*, Vol. 114, No. 4, 1992, pp. 657–666.

[8]Ling, W., Chung, J. N., Troutt, T. R., and Crowe, C. T., "Direct Simulation of a Three-Dimensional Temporal Mixing Layer with Particle Dispersion," *Journal of Fluid Mechanics*, Vol. 358, 1998, pp. 61–85.

[9]Crowe, C. T., Chung, J. N., and Troutt, T. R., "Particle Mixing in Free Shear Flows," *Progress in Energy and Combustion Science*, Vol. 14, No. 3, 1988, pp. 171–194.

[10]Wang, L. P., Tong, X. L., and DeSpirito, J., "Two-Way Coupled Particle-Laden Mixing Layer. Part 2: Non-Linear Evolution," 3rd International Conf. on Multiphase Flow, ICMF'98, Lyons, France, June 1998.

[11]Miller, R. S., and Bellan, J., "Direct Numerical Simulation of a Confined Three-Dimensional Gas Mixing with One Evaporating Hydrocarbon-Droplet-Laden Stream," *Journal of Fluid Mechanics*, Vol. 384, 1999, pp. 293–338.

[12]Thevand, N., and Daniel, E., "Linear Instability of Dilute Particle-Laden Compressible Mixing Layers," *Physics of Fluids*, Vol. 14, No. 1, 2002, pp. 392–402.

[13]Ishii, R., Umeda, Y., and Yuhi, M., "Numerical Analysis of Gas-Particle Two-Phase Flows," *Journal of Fluid Mechanics*, Vol. 203, 1989, pp. 475–515.

[14]Daniel, E., Saurel, R., Larini, M., and Loraud, J.-C., "A Multiphase Formulation for Two-Phase Flows," *International Journal of Numerical Methods for Heat and Fluid Flow*, Vol. 4, No. 3, 1994, pp. 269–280.

[15]Clift, R., Grace, J. R., and Weber, M. E., *Bubbles, Drops, and Particles*, Academic Press, New York, 1978.

[16]Knudsen, J. G., and Katz, D. L., *Fluid Mechanics and Heat Transfer*, Hemisphere, New York, 1958.

[17]Lumpp, T., and Guillard, H., Institut National de Recherche en Informatique et Automatique, INRIA Research Rept. 2217, Sophia-Antipolis, France, March 1994.

[18]Guillard, H., Malé, J. M., and Peyret, R., "Adaptative Spectral Methods with Application to Mixing Layer Computations," *Journal of Computational Physics*, Vol. 102, Sept. 1992, pp. 114–127.

[19]Thevand, N., Daniel, E., and Loraud, J. C., "On High Resolution Schemes for Solving Unsteady Compressible Two-Phase Dilute Viscous Flows," *International Journal for Numerical Methods in Fluids*, Vol. 31, No. 4, 1999, pp. 681–702.

[20]Thevand, N., "Contribution à l'Étude Numérique des Écoulements Instationnaires et Visqueux de Mélanges Gaz-Particules Dilués," Ph.D. Dissertation, Univ. Provence, Marseille, France, 1999.

[21]Zhang, D. Z., and Prosperetti, A., "Momentum and Energy Equations for Disperse Two-Phase Flows and Their Closure for Dilute Suspension," *International Journal of Multiphase Flow*, Vol. 23, No. 3, 1997, pp. 425–453.

[22]Wen, F., and Evans, J., "Effects of Particle Inertia on the Instability of a Particle-Laden Flow," *Computers and Fluids*, Vol. 25, No. 7, 1996, pp. 667–676.

[23]Jackson, T. L., and Grosh, C. E., "Inviscid Spatial Stability of a Compressible Mixing Layer," *Journal of Fluid Mechanics*, Vol. 208, 1989, pp. 609–636.

[24]Day, M. J., Mansour, N. N., and Reynolds, W. C., "Structure and Stability of Compressible Reacting Mixing Layers," Dept. of Mechanical Engineering, Rept. TF-75, Stanford Univ., Stanford, CA, Aug. 1999.

[25]Blumen, W., "Shear Layer Instability of an Inviscid Compressible Flow," *Journal of Fluid Mechanics*, Vol. 40, 1970, pp. 769–781.

[26]Gropengiesser, H., "Study on the Stability of Boundary Layers and Compressible Fluids," NASA Rept. TT F-12786, Feb. 1970.

[27]Chinzei, N. G., Masuya, T., Komuro, T., Murakami, A., and Kudou, K., "Spreading of Two-Stream Supersonic Turbulent Mixing Layers," *Physics of Fluids*, Vol. 29, No. 5, 1986, pp. 1345–1347.

[28]Papamoschou, D., and Roshko, A., "The Compressible Turbulent Shear Layer: An Experimental Study," *Journal of Fluid Mechanics*, Vol. 197, 1988, pp. 453–477.

J. Bellan
Associate Editor